Geochemistry, Geophysics, Geosystems®

Correspondence to:
C. S. Borlina,
cborlina@purdue.edu

Obtaining High-Resolution Magnetic Records From Speleothems Using Magnetic Microscopy

Cauê S. Borlina[1,2,3] ©, Eduardo A. Lima[3] ©, Joshua M. Feinberg[4] ©, Plinio Jaqueto[4] ©, Ioan Lascu[5] ©, Ricardo I. F. Trindade[6] ©, Eric Font[7] ©, Elisa M. Sánchez-Moreno[8] ©, Luca Antonio Dimuccio[9] ©, Yusuke Yokoyama[10] ©, Josep M. Parés[11], Benjamin P. Weiss[3] ©, and Jeffrey A. Dorale[12]

[1]Department of Earth, Atmospheric, and Planetary Sciences, Purdue University, West Lafayette, IN, USA, [2]Department of Earth and Planetary Sciences, Johns Hopkins University, Baltimore, MD, USA, [3]Department of Earth, Atmospheric and Planetary Sciences, Massachusetts Institute of Technology, Cambridge, MA, USA, [4]Department of Earth and Environmental Sciences, Institute for Rock Magnetism, University of Minnesota, Minneapolis, MN, USA, [5]Department of Mineral Sciences, National Museum of Natural History, Smithsonian Institution, Washington, DC, USA, [6]Instituto de Astronomia, Geofísica e Ciências Atmosféricas, Universidade de São Paulo, São Paulo, Brazil, [7]Departamento de Ciências da Terra, Universidade de Coimbra, Coimbra, Portugal, [8]Departamento de Física, EPS, Universidade de Burgos, Burgos, Spain, [9]University of Coimbra, Centre of Studies in Geography and Spatial Planning (CEGOT), Coimbra, Portugal, [10]Atmosphere and Ocean Research Institute, The University of Tokyo, Bunkyo City, Japan, [11]Centro Nacional de Investigación sobre la Evolución Humana, Burgos, Spain, [12]Department of Earth and Environmental Sciences, University of Iowa, Iowa, IA, USA

Abstract Speleothems are mineral deposits capable of recording detrital and/or chemical remanent magnetization at annual timescales. They can offer high-resolution paleomagnetic records of short-term variations in Earth's magnetic field, crucial for understanding the evolution of the dynamo. Owing to limitations on the magnetic moment sensitivity of commercial cryogenic rock magnetometers ($\sim 10^{-11}$ Am^2), paleomagnetic studies of speleothems have been limited to samples with volumes of several hundreds of mm^3, averaging tens to hundreds of years of magnetic variation. Nonetheless, smaller samples (~ 1–10 mm^3) can be measured using superconducting quantum interference device (SQUID) microscopy, with a sensitivity better than $\sim 10^{-15}$ Am^2. To determine the application of SQUID microscopy for obtaining robust high-resolution records from small-volume speleothem samples, we analyzed three different stalagmites collected from Lapa dos Morcegos Cave (Portugal), Pau d'Alho Cave (Brazil), and Crevice Cave (United States). These stalagmites are representative of a range of magnetic properties and have been previously studied with conventional rock magnetometers. We show that by using SQUID microscopy we can achieve a five-fold improvement in temporal resolution for samples with higher abundances of magnetic carriers (e.g., Pau d'Alho Cave and Lapa dos Morcegos Cave). In contrast, speleothems with low abundances of magnetic carriers (e.g., Crevice Cave) do not benefit from higher resolution analysis and are best analyzed using conventional rock magnetometers. Overall, by targeting speleothem samples with high concentrations of magnetic carriers we can increase the temporal resolution of magnetic records, setting the stage for resolving geomagnetic variations at short time scales.

Plain Language Summary Earth has a magnetic field that is generated in the outer core, and through paleomagnetism we can retrieve information about the evolution of the field from rocks. Different types of rocks have been used to determine how Earth's magnetic field has changed over time. In this study, we use magnetic microscopy to analyze the magnetic record of speleothems, which are rocks that form inside caves and that can record magnetic fields in annual scales. This allows us to obtain magnetic records with higher resolution than previous studies. This is important because Earth's magnetic field changes in timescales ranging from thousands of years to a few years, and obtaining records from speleothems using magnetic microscopy can help us track these variations. We provide data demonstrating how the technique can be used and showing its limitations, and we discuss how the geologic context of the cave influences the robustness of the magnetic record. We also provide protocols for future studies using magnetic microscopy in speleothems.

1. Introduction

Speleothems are mineral deposits formed in caves by dripping, pooling, or seeping water containing dissolved ions and mineral grains from the host bedrock and overlying soils. Because speleothems typically precipitate at

annual rates, they may preserve magnetic and environmental records with an exceptionally high temporal resolution, making them important targets for environmental magnetic and paleomagnetic studies (e.g., Feinberg et al., 2020; Font et al., 2014; Fu et al., 2021; Jaqueto et al., 2022; Lascu & Feinberg, 2011; Lascu et al., 2016; Latham et al., 1979; Morinaga et al., 1989; Strauss et al., 2013; Trindade et al., 2018; Zhu et al., 2012, 2017).

Speleothems can acquire detrital remanent magnetization (DRM) or chemical remanent magnetization (CRM) through embedded minerals such as magnetite, hematite, and goethite (Font et al., 2014; Strauss et al., 2013). While previous studies have targeted speleothems for paleomagnetism (e.g., Jaqueto et al., 2022; Lascu et al., 2016; Latham et al., 1979, 1989; Morinaga et al., 1985, 1989; Ponte et al., 2018; Sánchez-Moreno et al., 2022; Trindade et al., 2018), the temporal resolution of those records is limited by two main factors: (a) the sensitivity of the magnetometers used to obtain the magnetic measurements, and (b) the intensity of the sample's magnetization, which depends on the abundance of magnetic minerals and/or the strength of the magnetic field present when the magnetic record was acquired. The latter is of particular interest because statistical uncertainties and deviations in magnetic measurements are inversely related to the abundance of magnetic minerals in a sample (Berndt et al., 2016).

The development of superconducting quantum interference device (SQUID) microscopy for room-temperature geological samples (Egli & Heller, 2000; Fischer et al., 2014; Fong et al., 2005; Lima & Weiss, 2016; Oda et al., 2016; Weiss et al., 2007) has greatly improved magnetic field and moment sensitivities, allowing for measuring magnetic moments as low as $\sim 10^{-15}$ Am^2 (Lima & Weiss, 2016). Such sensitivity allows for measurements of previously inaccessible speleothem samples whose magnetic moments lie below the detection limit of commonly used rock magnetometers. Because the volume of the samples and the temporal resolution of the magnetic records are coupled, SQUID microscopy enables the retrieval of magnetic moment information from shorter time intervals. This approach can be used to identify rapid variations of Earth's magnetic field, providing constraints on the behavior of these variations, which in turn can be used to better understand the mechanisms responsible for driving short-term variations in Earth's dynamo such as jerks, spikes, excursions and reversals. Magnetic records from shorter time intervals can also allow for retrieving high-resolution paleoenvironmental records from speleothems. However, such improvement involves longer measurement times and more complex data processing required for obtaining magnetic moment information from magnetic microscopy data when compared to conventional magnetometry. Thus, it is important to establish for which speleothems it is advantageous to use this technique and how to maximize its capabilities.

Here, we conduct the first systematic study of paleomagnetic records preserved in discrete small-volume samples of speleothems using SQUID microscopy. We focus on three stalagmites from different locations: Lapa dos Morcegos Cave, Portugal; Pau d'Alho Cave, Brazil; and Crevice Cave, United States. To validate our technique, we use speleothems that have already been measured using traditional paleomagnetic techniques, which allows us to determine the robustness of the paleomagnetic records obtained with SQUID microscopy and establish how it can improve on conventional magnetometry results. Additionally, these speleothems are representative of different magnetic mineral abundances. We show that, by using SQUID microscopy, we can obtain robust paleomagnetic records with a five-fold increase in temporal resolution for some speleothems. We demonstrate how variations in the concentration of magnetic minerals along a speleothem may affect the temporal resolution and robustness of the magnetic record. We also propose new protocols for future high-resolution paleomagnetic studies of speleothems using magnetic microscopy.

2. Methods

2.1. Speleothem Samples

Stalagmites collected from three different locations were selected for this study. First, we selected a speleothem from Lapa dos Morcegos Cave, Portugal (henceforth identified as LM). We analyzed a sub-sample that contained magnetic records from 13 to 17 thousand of years (ka) ago (Figure 1a). We provide below details on carbon-dating method used to obtain ages from this speleothem. The LM stalagmite is composed of calcite and it was oriented in situ using a magnetic compass. For the present study, we analyzed samples from the top of the stalagmite ($\sim$3 cm), while data from the rest of the samples will be reported in the future. Samples analyzed with a superconducting rock magnetometer had a thickness of $\sim$4 mm and a total volume of $\sim$1,600 mm^3 that corresponds to averaging a couple hundred years of magnetic field variation.
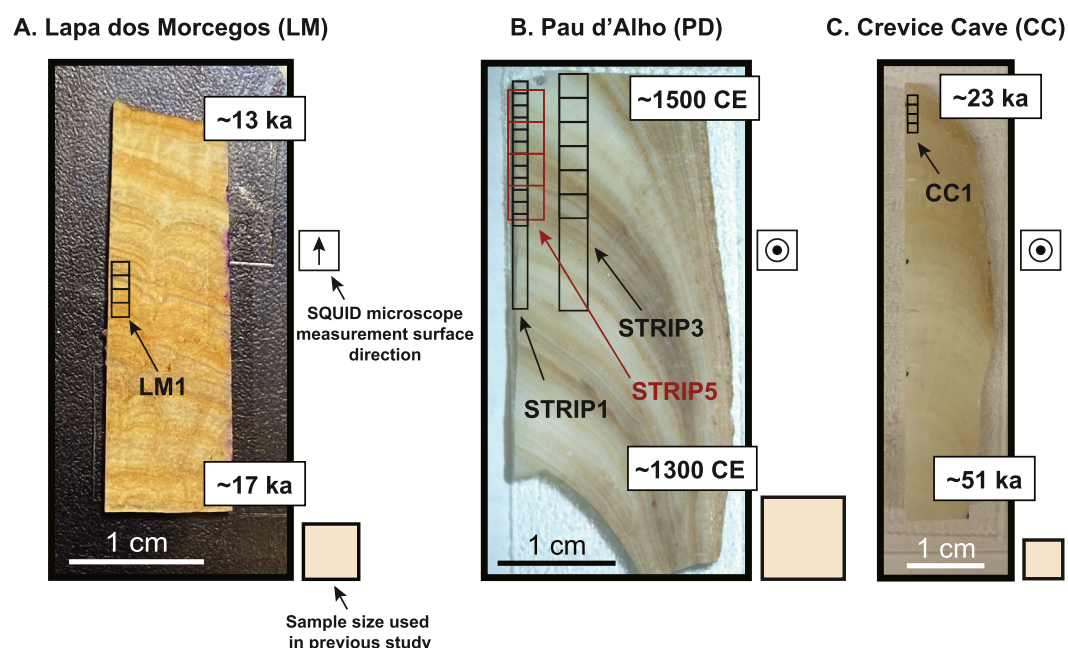
Figure 1. *Images of the speleothems analyzed in this study.* Shown are the thick sections along with the longitudinal strips extracted from speleothems from (a) Lapa dos Morcegos Cave, (b) Pau d'Alho Cave and (c) Crevice Cave. The squares across the longitudinal strips indicate how the samples were cut. The boxes on the lower right side of each sample show the approximate size of the samples used in previous paleomagnetic measurements of the samples. The box to the center right indicate the direction of the surface used to obtain the superconducting quantum interference device (SQUID) microscope magnetic maps.

Second, we analyzed a speleothem from the Pau d'Alho Cave System, Brazil (henceforth identified as PD). Previous work by Trindade et al. (2018) studied two speleothems (ALHO 06 and ALHO 31), which have overlapping magnetic records from the last ~1,600 years. These speleothems are mainly composed of calcite, with a complete mineralogical description found in Jaqueto et al. (2016). ALHO 31 was oriented in situ with a magnetic compass, while ALHO 06 had its orientation estimated by matching its declination record to field models for the same age interval. Ages for the PD samples were obtained using the U-Th method and layer counting (Novello et al., 2016; Trindade et al., 2018). We focused on a section from ALHO 06 that was available from the previous study and contained magnetic records between the years 1500 and 1600 CE (Figure 1b). Trindade et al. (2018) measured samples with a thickness of ~7 mm and a total volume of ~1,900 mm^3, which corresponds to averaging about 45 years of magnetic field variation.

Third, we studied a stalagmite from Crevice Cave, Missouri, United States (henceforth identified as CC). This speleothem was previously analyzed by Lascu et al. (2016) and provided records of the Laschamp excursion. The speleothem was originally collected for climate studies and was not oriented in the field. The total speleothem length was ~20 cm and contained magnetic records between 65 and 25 thousands of years (ka) ago (Figure 1c). Ages were obtained using the U-Th method and annual layer counting was anchored to the U-Th age depth curve. Lascu et al. (2016) analyzed samples with a thickness of 4–5 mm and a total volume of ~595 mm^3 that corresponded to averaging approximately one thousand years of magnetic field variation. Given that all three samples were previously studied using superconducting rock magnetometers, the measurements in this study were carried out on speleothem sections adjacent to the central part used in those studies, with varying degrees of layer curvature present. We discuss later the potential effects of the curvature to the magnetic record of a speleothem sample.

2.2. Sample Preparation

We prepared our samples in the Massachusetts Institute of Technology (MIT) Paleomagnetism Laboratory inside a positive-pressure shielded room to minimize contamination (field <200 nT). Samples were cut using a precision diamond wire saw (0.2 mm diameter wire) with deionized water as a cooling fluid.
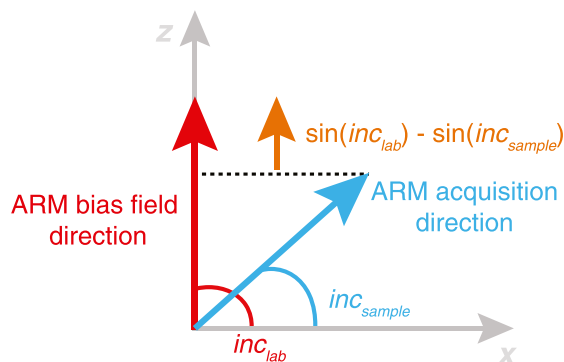
Figure 2. *Diagram showing how the ΔARM is calculated.* The red arrow indicates the applied field direction, inc_{lab}, and the blue arrow indicates the angle associated with the direction of the anhysteretic remanent magnetization (ARM) acquisition by the sample, inc_{sample}. The ΔARM parameter quantifies the average difference between these two directions across multiple ARM applications.

For LM, we obtained a ∼2 mm-thick longitudinal section (Figure 1a) from which we cut a 2-mm wide strip named LM1. We then obtained four samples with volumes of 3.2 mm^3 each (LM1.1–LM1.4) by cutting rectangular prisms measuring ∼0.8 × 2 × 2 mm. The samples were cut at every 1 mm along the growth axis, and the 0.8-mm dimension is the effective thickness of the pieces accounting for losses of material in the cutting process. Each sample produced magnetic records of a few decades each.

For PD, we obtained two ∼1 mm-thick longitudinal sections from ALHO 06 (Figure 1b). From one thick section we cut two strips, STRIP1 (S1, 1-mm wide), and STRIP3 (S3, 2-mm wide) (Figure 1b). From the second thick section, we obtained one strip, STRIP5 (S5, 2.7-mm wide). Following these initial cuts, we obtained samples shaped as rectangular prisms measuring ∼1 × 1 × 1 mm = 1 mm^3 (from S1), ∼2 × 2 × 1 mm = 4 mm^3 (from S3) and ∼2.7 × 2.7 × 1 mm = ∼7 mm^3 (from S5). The 1 mm^3 samples averaged the magnetic field in intervals of ∼5 years, the 4 mm^3 samples averaged the magnetic field in intervals of ∼10 years and the 7 mm^3 samples averaged the magnetic field in intervals of ∼20 years. We obtained 12 samples from S1 (S1.1–S1.12), 6 samples from S3 (S3.1–S3.6) and 4 samples from S5 (S5.1–S5.4).

For CC, we obtained a ∼1 mm-thick longitudinal section (Figure 1c), from which we cut a strip named CC1 which was 1-mm wide. We then obtained four samples with volumes of 1.2 mm^3 each (CC1.1–CC1.4) obtained by cutting rectangular prisms measuring ∼1 × 1.2 × 1 mm. Each 1.2 mm^3 volume averaged the magnetic field in intervals of ∼200 years.

We used cyanoacrylate cement to attach a glass cover slip to S1 prior to sub-sampling to facilitate handling, orienting, and gluing of samples, following the protocol of Borlina et al. (2021) to orient small samples. For the remaining samples, we used a nonmagnetic permanent marker to help orient the samples. All samples were glued to non-magnetic quartz disks using cyanoacrylate cement and were kept mutually oriented within 5–10° during the paleomagnetic measurements. We also note that the main section and the samples from S1 were obtained by using recirculating water from the speleothem during the cutting with the diamond wire saw, while the other samples were obtained by dripping fresh deionized water during the cutting process. We explore the potential importance of this in the discussion section.

2.3. Dating the Lapa dos Morcegos Speleothem

Because the age range spanned by the LM speleothem has not yet been reported in the literature, we present a summary of the methodology used for dating. Owing to LM's high detrital content, ages from the LM samples were obtained using ^{14}C dating. Radiocarbon analyses were performed with a single-stage accelerator mass spectrometer (AMS) at the Atmosphere and Ocean Research Institute of the University of Tokyo (Yokoyama et al., 2019). Approximately 10 mg of speleothem samples were cut, and cleaned with sonicated water and weak acid (Yokoyama et al., 2022). They were then graphitized for radiocarbon dating using the method described by Yokoyama et al. (2007), prior to the ^{14}C analysis by AMS. ^{14}C ages were calibrated to calendar years using the calibration software Oxcal v4.4.4 (Ramsey, 2009) with the IntCal20 data set (Reimer et al., 2020).

2.4. Rock Magnetism

We obtained first-order reversal curve (FORC) measurements for a few samples of PD and LM to characterize the coercivity distributions, domain states, and magnetostatic interactions of magnetic minerals for samples that exhibited distinct magnetic behavior. We selected two S3 samples (S3.1 and S3.5) and two LM1 samples (49 and 52). FORCs from the samples S3.1 and S3.5 were obtained using an 8604 Lake Shore Cryotronics Vibrating Sample Magnetometer at the Smithsonian National Museum of Natural History. For each sample, we collected 141 FORCs using a 300 mT saturation field with B_c (coercivity) ranging from 0 to 80 mT and B_u (interaction field) ranging from −20 to 40 mT. The field increment was 1 mT and the measurement averaging time was 3 s for S3.5 and 6 s for S3.1. FORCs from the samples LM1.49 and LM1.52 were obtained using a MicroMag 3900 Vibrating Sample Magnetometer at the Archaeomagnetism Laboratory in the Centro Nacional de Investigación sobre la Evolución
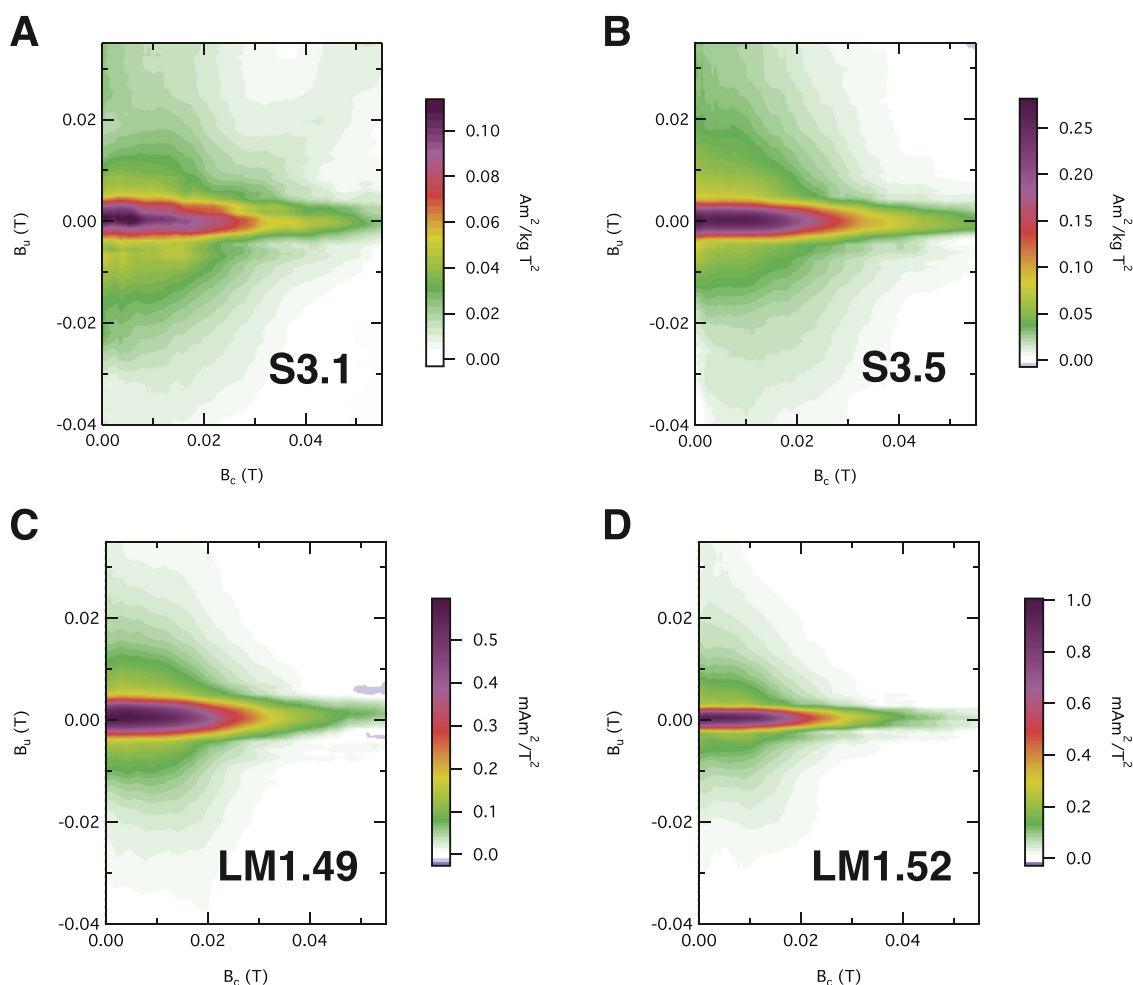
Figure 3. *First-order reversal curve (FORC) diagrams for select PD and LM samples*. FORC diagrams for samples (a) S3.1, (b) S3.5, (c) LM1.49, and (d) LM1.52. All four samples exhibit similar features on the FORC diagrams, indicating the presence of single-domain and vortex state magnetic carriers. The difference in signal strength between samples from the same speleothem coupled with the overall similarity of features in the FORCs indicate that the concentration of magnetic carriers varies across the samples.

Humana. For these samples, we collected 130–210 FORCs using a 500 mT saturation field with B_c ranging from 0 to 80 mT and B_u ranging from −50 to 50 mT. The field increment was 0.9–1.5 mT and the measurement averaging time was 0.5–1 s. FORCs were processed and FORC diagrams generated using FORCinel 3.07 (Harrison & Feinberg, 2008), with the VARIFORC variable smoothing protocol (Egli, 2013). We used the following smoothing parameters for the FORCs: $s_{c,0} = 24$, $s_{b,0} = 11.5$, $s_{c,1} = s_{b,1} = 24$, $\lambda = 0.125$ (PD S3.1); $s_{c,0} = 19$, $s_{b,0} = 9.5$, $s_{c,1} = s_{b,1} = 19$, $\lambda = 0.125$ (PD S3.5); and $s_{c,0}16$, $s_{b,0} = 7$, $s_{c,1} = s_{b,1} = 16$, $\lambda = 0.15$ (LM samples).

2.5. Paleomagnetism

For the LM samples, initial natural remanent magnetization (NRM) measurements and alternating field (AF) demagnetization of bulk LM samples were conducted at the Laboratory of Paleomagnetism of the University of Burgos using a 2G Enterprises Superconducting Rock Magnetometer and a 3-axis degausser system. For the PD samples, bulk sample measurements are described in Trindade et al. (2018), whereas bulk sample measurements of the CC speleothem are described in Lascu et al. (2016). All remaining measurements were performed at the MIT Paleomagnetism Laboratory using a SQUID microscope (Weiss et al., 2007) in combination with an automatic 3-axis degausser system (Kirschvink et al., 2008). AF demagnetization was conducted in 5 mT steps up to 50 mT. Prior to cutting the thick section into strips and sub-samples, we mapped the NRM of the thick sections using the SQUID microscope. Maps of the z-component (normal to the sample's top surface) of the NRM were
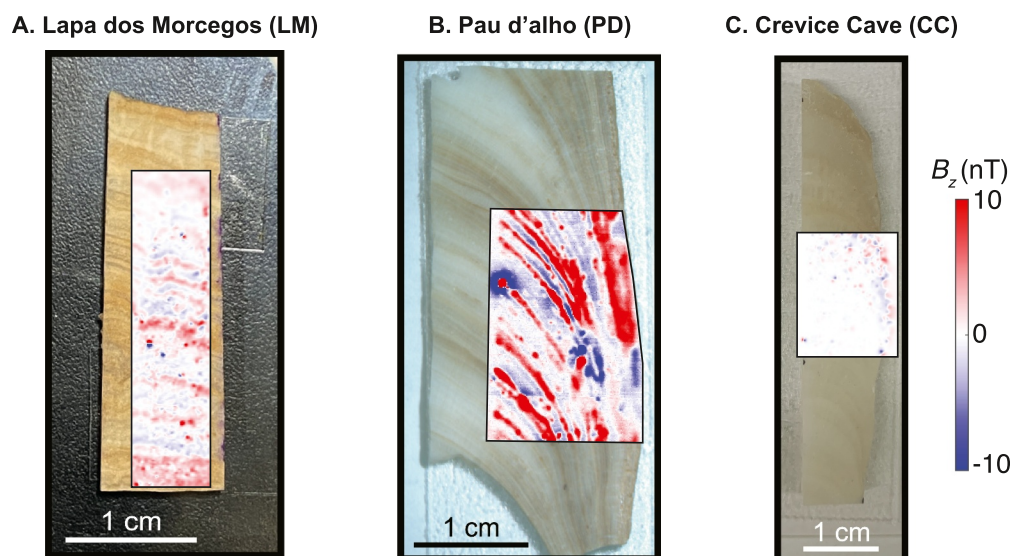
Figure 4. *Overlay of superconducting quantum interference device (SQUID) microscopy maps on images for the three stalagmites analyzed here*. Out-of-the-page magnetic field component (B_z) maps were measured ~200 μm above the samples. Color scale on the right is the same for all three samples. We notice strong correlation between the strength of the remanent magnetic field and the darkness of speleothem bands for samples from (a) Lapa dos Morcegos Cave (LM) and (b) Pau d'Alho Cave (PD), indicating layers that are rich in magnetic minerals. We do not observe such pattern in the thick section from (c) Crevice Cave (CC), suggesting a lower concentration of magnetic minerals in this sample.

obtained at an effective sensor-to-sample distance of ~300 μm inside a magnetically shielded room. We retrieved magnetic moments from the SQUID microscopy maps by using the inversion technique described in Lima et al. (2023). PD and CC samples were mapped parallel to their growth direction and the corresponding magnetic moments were rotated to match the direction of the growth axis, while LM samples were mapped perpendicular to the growth axis (Figure 1). The directions of NRM components were calculated using principal component analysis (PCA) (Kirschvink, 1980). If a NRM component had a deviation angle less than the maximum angular deviation (MAD), then this component was inferred to be the characteristic component and therefore anchored to the origin (Kirschvink, 1980; Tauxe & Staudigel, 2004).

Following the completion of the AF demagnetization sequence, we applied a series of repeated anhysteretic remanent magnetization (ARM) steps to each sample to establish the robustness of the magnetic records retrieved. The accuracy and precision of these ARM applications are useful for determining whether the concentration of magnetic minerals in each individual sample is sufficiently high to acquire a magnetization in the direction of an applied field. We use the ARM as a proxy for the DRM and/or CRM of the speleothems, an assumption that supported by paleointensity studies with speleothems (Ponte et al., 2018). We conducted five independent ARM applications for each sample. To quantitatively determine how well a sample can acquire magnetization direction, we calculated the ΔARM parameter (Figure 2), defined as:

$$\Delta ARM = \frac{1}{2}\sqrt{\frac{1}{N}\sum_{i=1}^{N}\left[\sin(inc_{lab}) - \sin(inc_{sample,i})\right]^2},$$

(1)

where N is the number of ARM applications, inc_{lab} is the expected inclination of the application of the ARM along the z-axis (i.e., $inc_{lab} = 90°$ or $inc_{lab} = -90°$), and $inc_{sample,i}$ is the measured magnetic inclination of the sample's remanence after ARM application i out of N. The 0.5 factor in front of the expression normalizes the parameter between 0 and 1. The ΔARM parameter accounts for both systematic deviations (e.g., magnetic anisotropy) and random deviations (e.g., scatter in the magnetization acquisition) from the expected direction and provides an estimation of how well a sample can acquire magnetic direction. For $inc_{lab} = -90°$, a value of $\Delta ARM = 0$ indicates that all ARM acquisitions are in the same direction as the ARM application, while an $\Delta ARM = 1$ indicates that all the ARM acquisitions are in the opposite direction from the ARM application. For reference, five

Table 1
Summary of Components From Alternating Field Demagnetization From LM Samples

Sample	Component	Range (mT)	Declination (°)	Inclination (°)	MAD (°)	DANG (°)	Anchored?
LM.1	LC	0–5	34.5	−51.8	–	–	–
	HC	5–25	301.3	62.5	5.1	3.3	Y
LM.2	HC	0–32	308.3	52.1	7.8	17.9	Y
LM.3	LC	0–5	335.7	−6.3	–	–	–
	HC	5–40	322.7	55.2	7.6	16.9	N
LM.4	LC	0–40	314.4	53.9	8.6	8.0	Y

Note. The first column lists the sample name, the second column lists the name of the component (LC for low coercivity and HC for high coercivity), the third column lists the range used to calculate the fit in mT, the fourth, fifth and sixth columns show the results of the principal component analysis, which include the declination, inclination and maximum angular deviation (MAD), the seventh column lists the deviation angle (DANG) for the component, and the eighth column denotes whether the component is anchored (Y for yes and N for no).

measured ARM applications that are either systematically 25° off the correct ARM direction or have a 25° scatter around the correct direction will have $\Delta ARM \sim 0.047$. Ultimately, the choice of the bias field used to calculate the ΔARM will depend on the expected strength of the intensity of the paleomagnetic field. For instance, some of the

Table 2
Summary of Components From Alternating Field Demagnetization From S1 Samples

Sample	Component	Range (mT)	Declination (°)	Inclination (°)	MAD (°)	DANG (°)	Anchored?
S1.1	LC	0–5	104.1	−29.1	16.8	–	–
	HC	5–22.5	324.2	6.7	5.8	3	Y
S1.2	LC	0–2.5	97.1	56.7	–	–	–
	HC	5–22.5	85.5	60.4	14.8	7.4	Y
S1.3	LC	0–2.5	80	10.9	–	–	–
	HC	2.5–35	99.6	−20.9	39	98.2	N
S1.4	LC	0–15	223.2	40.5	29.3	–	–
	HC	15–47.5	108.7	−3.3	44.4	71.5	N
S1.5	LC	0–5	166.4	−49.4	9.4	–	–
	HC	5–30	345.1	68.2	21.8	28.1	N
S1.6	LC	0–2.5	65.9	3.9	0	–	–
	HC	2.5–30	20.7	20.3	18.7	28.9	N
S1.7	LC	0–7.5	282.2	−41.7	17.6	–	–
	HC	7.5–27.5	40.1	−4.4	13	15.3	N
S1.8	LC	0–5	301.3	38.7	15.2		–
	HC	5–20	19.5	−18.9	25.9	23.9	Y
S1.9	HC?	0–30	249.8	12.8	28.1	115.7	N
S1.10	LC	0–25	350.6	−34	35.3	–	–
	HC	25–45	154.6	12.1	22.6	24.7	N
S1.11	HC	0–30	28.2	−39.7	44.3	55.9	N
S1.12	LC	0–7.5	189.5	18.1	28.3	–	–
	HC	7.5–17.5	346	33.7	8.9	41.4	N

Note. The first column lists the sample name, the second column lists the name of the component (LC for low coercivity and HC for high coercivity), the third column lists the range used to calculate the fit in mT, the fourth, fifth and sixth columns show the results of the principal component analysis, which include the declination, inclination and maximum angular deviation (MAD), the seventh column lists the deviation angle (DANG) for the component, and the eighth column denotes whether the component is anchored (Y for yes and N for no).

Table 3
Summary of Components From Alternating Field Demagnetization From S3 Samples

Sample	Component	Range (mT)	Declination (°)	Inclination (°)	MAD (°)	DANG (°)	Anchored
S3.1	HC?	0–50	130.8	−30.7	45.7	161.2	N
S3.2	LC	0–5	97.2	−42.2	–	–	–
	HC	10–25	43.3	9.1	35.5	39.9	–
S3.3	LC	0–10	30.9	19.3	20	–	–
	HC	20–30	347.1	−22.1	34.3	38.7	N
S3.4	LC	0–5	88.1	41.8	0	–	–
	HC	5–50	18.5	−1.1	9.4	8.4	Y
S3.5	LC	0–10	180.8	42	9.6	–	–
	HC	10–50	6	−2.4	7.5	3.6	Y
S3.6	LC	0–10	341.6	27.7	4.3	–	–
	HC	10–45	14.5	−20	28.1	32.9	N

Note. The first column lists the sample name, the second column lists the name of the component (LC for low coercivity and HC for high coercivity), the third column lists the range used to calculate the fit in mT, the fourth, fifth and sixth columns show the results of the principal component analysis, which include the declination, inclination and maximum angular deviation (MAD), the seventh column lists the deviation angle (DANG) for the component, and the eighth column denotes whether the component is anchored (Y for yes and N for no).

studied speleothems contain records of the South Atlantic Anomaly and of magnetic excursions, and we chose to use a 30 µT bias field to more accurately assess the recording capabilities of the speleothems during such events. For times when the geomagnetic field is stronger, this lower bias field places an upper limit on the directional error of these samples.

3. Results

The FORC diagrams of the two PD samples from S3 show similar features, but with S3.5 having a signal strength more than twice that of S3.1 (Figures 3a and 3b). Both FORC diagrams have a low-coercivity central ridge along the horizontal axis characteristic of non-interacting single domain (SD) particles (<0.1 µm) (Harrison & Lascu, 2014). The central ridge coercivity distribution spans the interval 0–65 mT, with a peak amplitude near the origin. The background signal, with increasing spread closer to the vertical axis, is typical of <0.1–5 µm-sized particles in the pseudo-single domain state characterized by single vortex and multivortex configurations (Lascu et al., 2018; Roberts et al., 2017). Similar results are observed in the FORC diagrams from the samples obtained from LM1 (Figures 3c and 3d). The FORCs from the LM1 samples show the central ridge like those from the S3

Table 4
Summary of Components From Alternating Field Demagnetization From S5 Samples

Sample	Component	Range (mT)	Declination (°)	Inclination (°)	MAD (°)	DANG (°)	Anchored?
S5.1	NA	0–50	224.6	60.4	20	–	–
S5.2	LC	0–10	247.1	−65.8	12	–	–
	HC	10–50	65	56.2	11.9	21.8	N
S5.3	LC	0–5	102.1	−3.4	–	–	–
	HC	10–35	48.7	−34.3	18	69.5	N
S5.4	LC	0–5	156.9	−37.6	–	–	–
	HC	5–30	114.7	−52.9	33	80.4	N

Note. The first column lists the sample name, the second column lists the name of the component (LC for low coercivity and HC for high coercivity), the third column lists the range used to calculate the fit in mT, the fourth, fifth and sixth columns show the results of the principal component analysis, which include the declination, inclination and maximum angular deviation (MAD), the seventh column lists the deviation angle (DANG) for the component, and the eighth column denotes whether the component is anchored (Y for yes and N for no).

Table 5
Summary of Components From Alternating Field Demagnetization From Crevice Cave Samples

Sample	Component	Range (mT)	Declination (°)	Inclination (°)	MAD (°)	DANG (°)	Anchored?
CC.1	–	0–50	326.1	17.1	35.1	76.2	–
CC.2	–	0–50	32.2	−39.1	30.8	113.7	–
CC.3	–	0–50	273.6	27	30.4	73.3	–
CC.4	–	0–50	17.2	−12.9	14.9	160.2	–

Note. The first column lists the sample name, the second column lists the name of the component (LC for low coercivity and HC for high coercivity), the third column lists the range used to calculate the fit in mT, the fourth, fifth and sixth columns show the results of the principal component analysis, which include the declination, inclination and maximum angular deviation (MAD), the seventh column lists the deviation angle (DANG) for the component, and the eighth column denotes whether the component is anchored (Y for yes and N for no).

samples, indicative of SD particles. The central ridge spans coercivities of 0–65 mT, similar to that of the S3 samples. The background signal is also similar to that of the S3 samples, indicating the presence of a vortex component. Because the masses of the LM samples were not measured, it is not possible to directly compare the intensity per unit mass between samples from PD and LM. The central ridge of LM1.52 appears narrower than that of the other samples because of the higher measurement resolution of this sample.

NRM field maps of the thick sections of each speleothem prior to cutting the longitudinal strips are shown in Figure 4. We observe that the PD thick section has the strongest magnetic field sources from all the sections, demonstrating clear correlation between dark bands and strong magnetic field signal. We also observe strong and weak magnetic signals alternating across the PD sample. A strong magnetic field signal is also observed on the edges of the PD thick section, where stalagmite layers merge. Compared to the PD sample, a less pronounced banding pattern in the magnetic signal is observed within the thick section of the LM stalagmite. In the LM thick
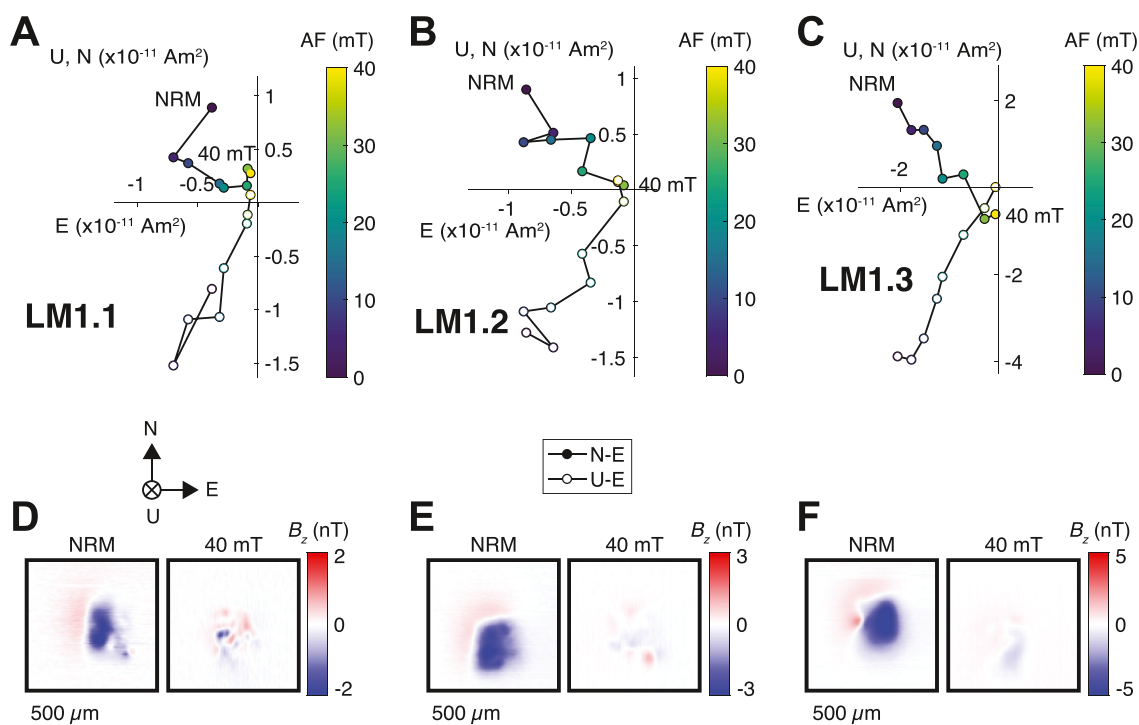
Figure 5. *Alternating field (AF) demagnetization of select Lapa dos Morcegos (LM) samples.* (a–c) Orthographic projections of natural remanent magnetization (NRM) vector endpoints during AF demagnetization. Closed symbols represent the north-east (N-E) projection of the magnetic moment and open symbols represent the up-east (U-E) projection of the magnetic moment. Color scales show the AF level. (d–f) Out-of-the-page magnetic field component (B_z) maps for select steps measured at a height of ∼300 μm above the samples obtained with the superconducting quantum interference device (SQUID) microscope. Coordinate system refers to measurements coordinates for the SQUID microscope maps.
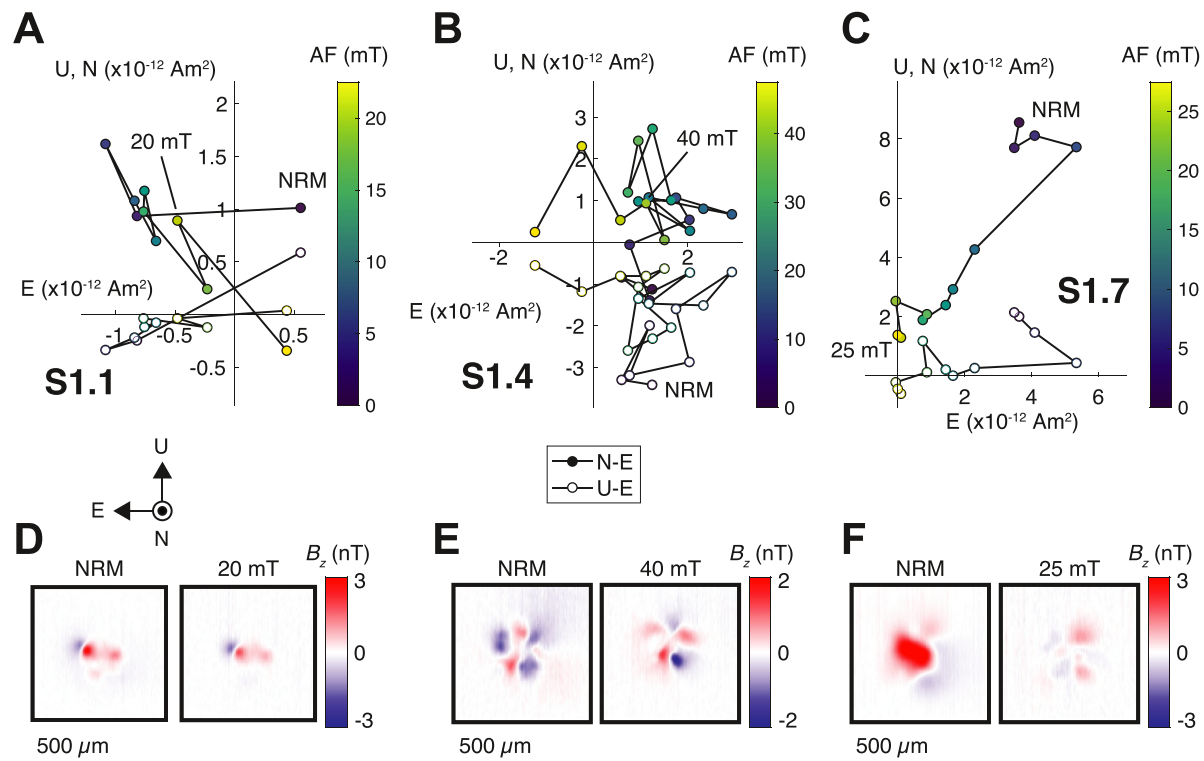
Figure 6. *Alternating field (AF) demagnetization of select Pau d'Alho (PD) STRIP1 samples.* (a–c) Orthographic projections of natural remanent magnetization (NRM) vector endpoints during AF demagnetization. Closed symbols show the north-east (N-E) projection of the magnetic moment and open symbols represent the up-east (U-E) projection of the magnetic moment. Color scales show the AF levels. (d–f) Out-of-the-page magnetic field component (B_z) maps for selected steps measured at a height of ~300 μm above samples obtained with the superconducting quantum interference device (SQUID) microscope. Coordinate system refers to measurements coordinates for the SQUID microscope maps.

section, we observe alternating layers of positive and negative fields, suggesting either rapid variations in the magnetic field recorded in the samples or weak regions of magnetic field signal that allow for fringing fields from strong magnetic bands to appear. The CC thick section shows the strongest signals on the edges of the sample, and we do not observe the clear banding associated with magnetic field signal across layers as identified in the other two speleothems. Overall, the magnetic signal of the CC samples is noticeably weaker than that of the other two speleothems.

AF demagnetization of the speleothem samples generally revealed two NRM components, usually with a low coercivity component between 5 and 10 mT and a high coercivity (HC) component between 20 and 50 mT. We summarize the PCA components of all samples in Tables 1–5. We also present select plots of the orthographic projections of NRM vector endpoints in Figures 5–9. Additionally, Figures 10–12 summarize the inclination, declination, MAD and ΔARM for our samples. All demagnetized samples from the LM stalagmite had components (Figures 5 and 10). PD samples showed more variability across sizes and samples, resulting in demagnetizations that ranged from noisy to origin-trending components (Figures 6–8, and 11). Finally, CC samples did not produce any discernible components during demagnetization (Figures 9 and 12).

We also report on the comparison between data sets obtained with traditional paleomagnetic techniques and those obtained here using the SQUID microscope. Figures 13 and 14 show this comparison for the measurements obtained from the LM and PD samples. We do not report the same comparison for the CC samples because of their lack of stable magnetic components observed in the SQUID microscopy measurement sequences.
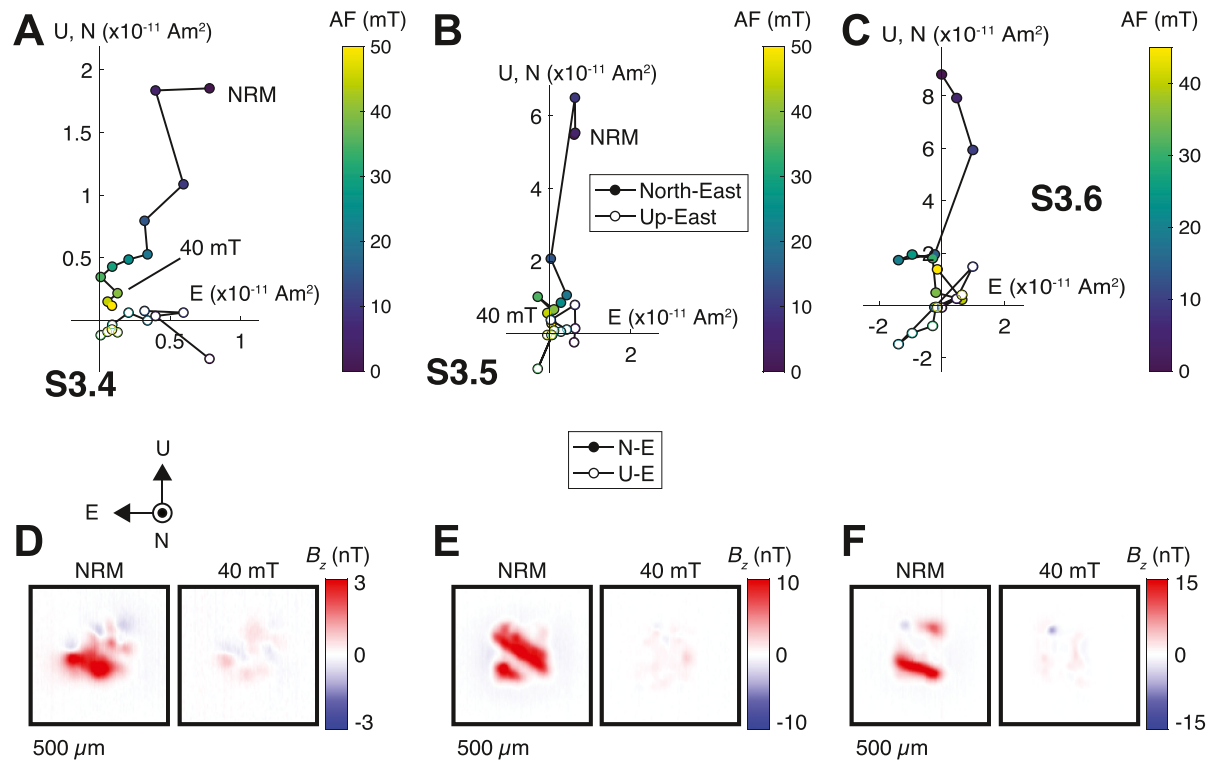
Figure 7. *Alternating field (AF) Demagnetization of selected Pau d'Alho (PD) STRIP3 samples*. (a–c) Orthographic projections of natural remanent magnetization (NRM) vector endpoints during AF demagnetization. Closed symbols show the north-east (N-E) projection of the magnetic moment and open symbols represent the up-east (U-E) projection of the magnetic moment. Color scales show the AF levels. (d–f) Out-of-the-page magnetic field component (B_z) maps for selected steps measured at a height of ∼300 μm above samples obtained with the superconducting quantum interference device (SQUID) microscope. Coordinate system refers to measurements coordinates for the SQUID microscope maps.

4. Discussion

4.1. Obtaining Magnetic Moments From Speleothem Samples

A distinctive aspect of this study is that, compared to previous studies of isolated zircon grains and chondrules (e.g., Borlina et al., 2020, 2021; Fu, Lima, & Weiss, 2014; Fu, Weiss, et al., 2014; Fu et al., 2017), speleothem samples exhibit predominantly non-dipolar fields in SQUID microscopy maps (Figures 5d–5f, 6d–6f, 7d–7f, 8d–8f, and 9d–9f). The non-dipolarity of the speleothem samples is likely associated with the nature of the magnetic acquisition process, the size of the samples and the fact that many of the magnetic sources are polymineralic assemblages of clays, oxides and organic matter. Overall, retrieving the net magnetic moment from speleothem samples using magnetic microscopy requires using multipolar inversion techniques (compare Lima et al. (2023) with Lima and Weiss (2016)).

4.2. Variability of Magnetic Properties Between Different Speleothems

From these speleothems we observed three different behaviors. First, the LM stalagmite section showed NRM homogeneity across samples, consistent with the overall homogenous magnetic intensity of the NRM of the thick section (Figure 4a) and the measured low ΔARM values (Figure 10d). We also observed well-constrained HC components during AF demagnetization (Figure 5), and excellent agreement between the data measured in larger volumes and those obtained with SQUID microscopy (13). Overall, these observations indicate that this stalagmite is an excellent target for future paleomagnetic studies with the goal of obtaining high-resolution temporal magnetic records. In fact, this sample can provide an improvement of at least 5 times in the temporal resolution of the magnetic record compared to that obtained with traditional paleomagnetic instrumentation.
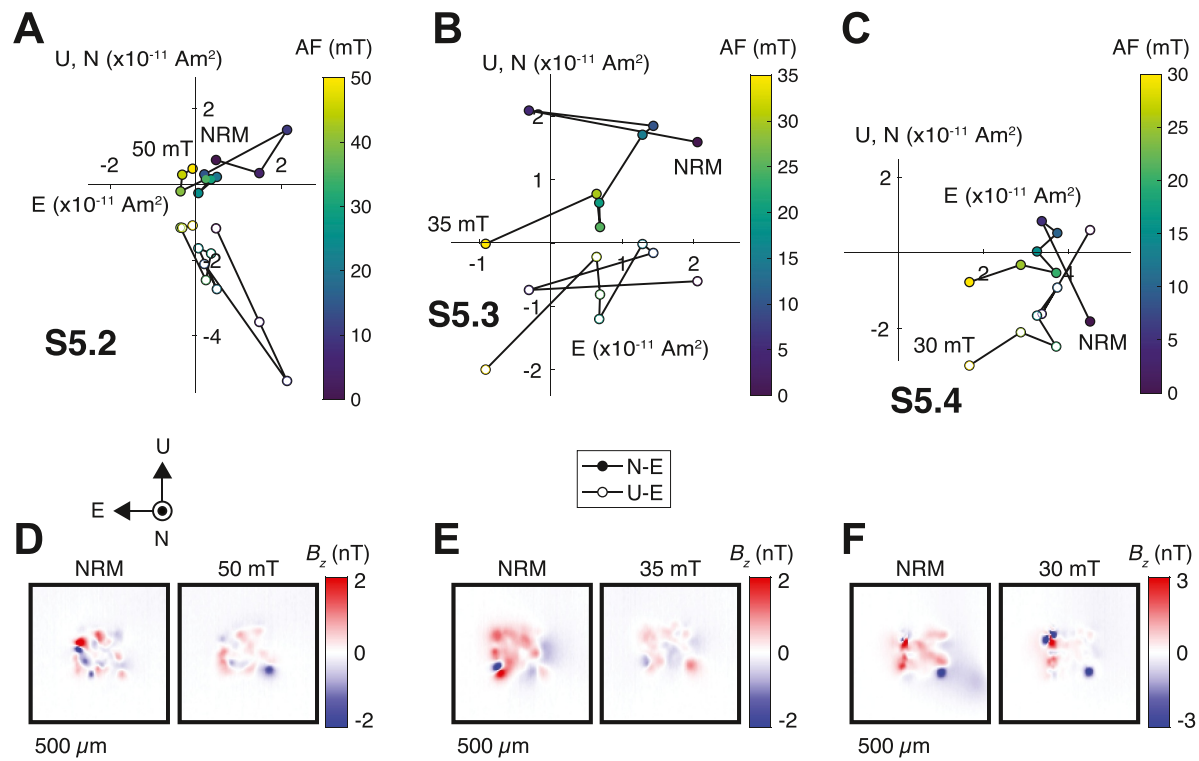
Figure 8. *Alternating field (AF) demagnetization of select Pau d'Alho (PD) STRIP5 samples.* (a–c) Orthographic projections of natural remanent magnetization (NRM) vector endpoints during AF demagnetization. Closed symbols show the north-east (N-E) projection of the magnetic moment and open symbols represent the up-east (U-E) projection of the magnetic moment. Color scales show the AF levels. (d–f) Out-of-the-page magnetic field component (B_z) maps for selected steps measured at a height of ~300 μm above samples obtained with the superconducting quantum interference device (SQUID) microscope. Coordinate system indicates the original direction of the measurements obtained with the SQUID microscope compared to the ones reported in the orthographic projections.

The second type is represented by the PD stalagmite, which showed variable magnetic properties along the growth axis. We observed large variations in the strength of the NRM field of the thick section that correlates with the banding seen in the image of the sample (Figure 4b) and the variations in the ΔARM parameter (Figures 11j–11l). These variations are further highlighted by the observation that some samples present HC components (e.g., Figures 6c, 7a, and 8a) while other samples do not show well-constrained components (e.g., Figures 6b and 8b). Similar variations are observed by comparing the results from this study to that of Trindade et al. (2018). The direction and its associated MAD from some samples include the data from Trindade et al. (2018) while others do not (Figure 14). In summary, the PD stalagmite has varying concentrations of magnetic minerals across the growth axis and if a uniform sampling size is employed for SQUID microscopy studies, some regions will produce reliable magnetic records while others might not. Nonetheless, the regions with strongest NRM signal indicating high concentration of magnetic minerals in this speleothem can help improve the current magnetic record by a factor of 2–3 times. Below, we discuss the effect of different sample sizes in the paleomagnetic results and how sample size can help produce more consistent and robust results in heterogeneous speleothems.

The third type is represented by the CC sample. This speleothem has a lower concentration of magnetic minerals as demonstrated by the very weak magnetic fields observed in the SQUID microscope NRM map (Figure 4c) and by the consistently high ΔARM values (Figure 12d). The lack of discernible NRM components (Figure 9) further indicates that this sample has poor recording properties at the small spatial scales associated with micro-paleomagnetic studies. Owing to the lower concentration of magnetic minerals, intrinsic to this speleothem, we observe that these samples do not have enough magnetic carriers to be analyzed in such small volumes, compared to that used by Lascu et al. (2016). Such speleothems can be more successfully studied using traditional bulk sample methods, but are not amenable to temporal resolution improvements from micro-paleomagnetic studies.
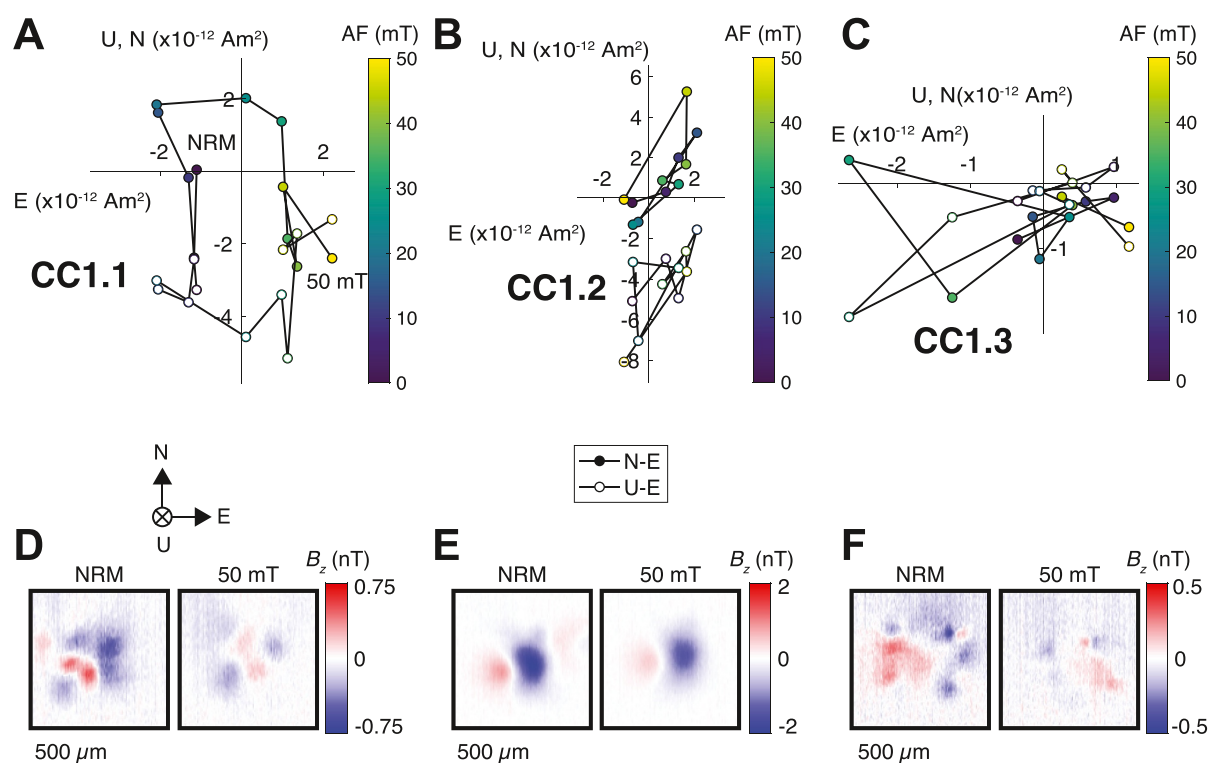
Figure 9. *Alternating field (AF) demagnetization of select Crevice Cave (CC) samples.* (a–c) Orthographic projections of natural remanent magnetization (NRM) vector endpoints during AF demagnetization. Closed symbols show the North-East projection of the magnetic moment and open symbols show Up-East projection of the magnetic moment. Color scales show the AF levels. (d–f) Out-of-the-page magnetic field component (B_z) maps for selected steps measured at a height of ~300 μm above samples obtained with the superconducting quantum interference device (SQUID) microscope. Coordinate system indicates the original direction of the measurements obtained with the SQUID microscope compared to the ones reported in the orthographic projections.

In summary, the three speleothems analyzed represent different examples in a range of magnetic properties of speleothems: (a) speleothems with magnetic properties similar to those of the CC speleothem do not benefit from high-resolution analysis, as the temporal resolution of their magnetic record cannot be meaningfully improved beyond that obtained with traditional paleomagnetic instrumentation; (b) speleothems like LM allow for an improvement in temporal resolution of the magnetic record by a factor of five or better; (c) speleothems like PD represent an intermediate example between those two endmembers, with regions of low concentration of magnetic carriers that may not benefit from high-resolution analysis, and others that allow for a meaningful temporal resolution improvement. Ultimately, we are limited by the characteristics of a given speleothem and not by the instrumental technique when obtaining high-temporal-resolution paleomagnetic records from speleothems: there must be enough magnetic carriers in a small-volume sample capable of statistically recording the magnetic field.

4.3. Variability of Magnetic Properties in Speleothems

4.3.1. Magnetic Mineralogy of a Heterogeneous Speleothem

Both PD and LM show variations in the amount of magnetic carriers across their growth axis with the variations being more pronounced in the PD sample (Figure 4). Magnetic variability in a speleothem can emerge from at least three scenarios: (a) the NRM is weak because Earth's magnetic field was weak during magnetic acquisition, (b) the concentration of magnetic minerals changes across the speleothem or (c) the composition of magnetic minerals changes across the speleothem. For the first case, the ΔARM parameter can help determine if the weak magnetization from a speleothem comes from the actual magnetic field of the Earth or from the magnetic properties of the sample. As discussed above, this is unlikely to be the case for the samples observed here. We now focus on the other two cases. The FORC analysis shown in Figure 3 from two PD samples (S3.1 and S3.5) helps differentiate between these two cases. The FORC diagram supports the presence of fine-grained magnetite and
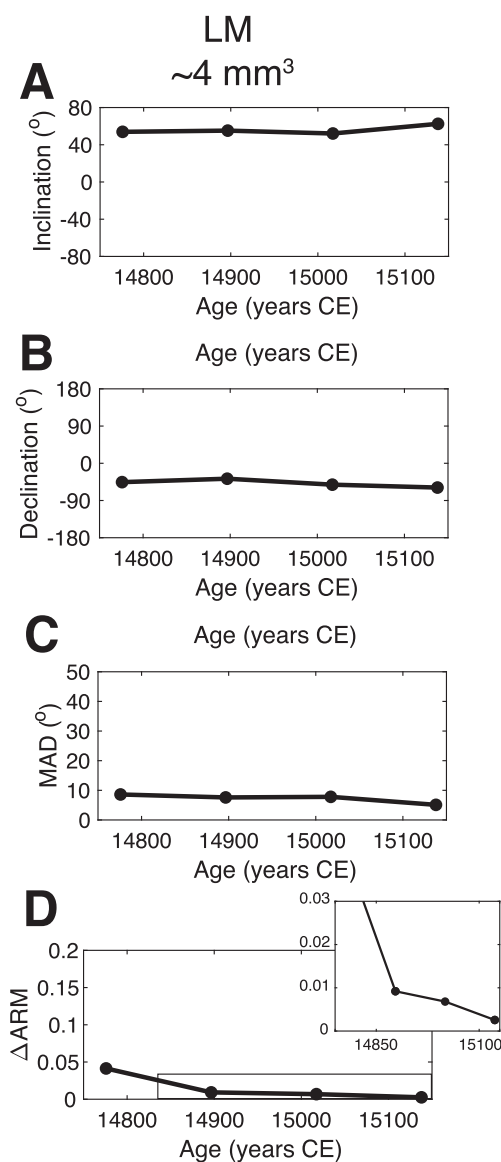
Figure 10. *Summary of magnetic directions, maximum angular deviation (MAD) and ΔARM values as a function of age for the Lapa dos Morcegos (LM) samples. Shown are plots for (a) inclination, (b) declination, (c) MAD and (d) ΔARM, including an inset of the ΔARM values.*

maghemite as the main magnetic carriers, similar to that reported by Trindade et al. (2018). Thus, the difference in signal strength between the FORCs is attributed to a difference in concentration of magnetic grains between the two samples, suggesting that S3.1 has smaller concentration of magnetic grains than S3.5. Additionally, sample S3.1 comes from the top part of the PD thick section (Figure 1b) which is predominately clear, compared to sample S3.5 which comes from the lower, darker regions of the stalagmite, richer in magnetic minerals as suggested by the FORC data. We also observed a higher ΔARM value for sample S3.1 ($\Delta ARM = 0.18$) compared to that of sample S3.5 ($\Delta ARM = 0.001$) further confirming that the coloring of the stalagmite layers may help determine which regions are enriched in detrital material, hence in magnetic minerals, resulting in better properties for paleomagnetic studies.

Overall, the observed correlation between dark bands in the PD thick section and magnetic strength (Figure 4b) together with the FORC data indicate that darker regions contain higher concentration of magnetic minerals than lighter regions of the speleothem and are likely to retain magnetic records with lower statistical error (see Fu et al. (2021) for a complete discussion on the potential source of the dark regions in this speleothem).

For the case of the CC sample, we note that previous work reported the presence of SD magnetite in these samples, similar to what we observe in PD and LM, further supporting that the concentration, not the mineralogy, is the main reason why a sample might not be ideal for micro-paleomagnetic work (Lascu et al., 2016).

4.3.2. The Effect of Sample Size on the Paleomagnetic Record

The larger samples (STRIP3 and STRIP5) are more stable during AF demagnetization (Figures 7 and 8) due to the higher content of magnetic minerals per sample that allows them to better average the small length-scale compositional variations. This results in a higher number of robust magnetic directions for samples from STRIP3 and STRIP5, supported by overall lower MADs and ΔARM, when compared to samples from STRIP1 (Figure 11).

Nonetheless, when we compare the data from STRIP1, STRIP3, and STRIP5 to results previously obtained by Trindade et al. (2018) (Figure 14) we observe that the best overall agreement between the data from this study to those of the previous study occurs for STRIP3 when the ΔARM is used to exclude samples from the data analysis. This suggests that somewhere in the size range (from 1 to 7 mm^3) there is an optimal size, in this case STRIP3 (~4 mm^3), that will yield consistently more robust paleomagnetic directions. This is likely associated with the non-dipolarity of these samples: as they get bigger in volume, the inversion needs to account for higher degrees/orders in the spherical harmonics expansion that are more affected by measurement noise that is commonly present in the field maps of the very weakly magnetized speleothems (Lima et al., 2023). In addition, larger samples require larger mapping areas and, ultimately, longer times for a complete micro-paleomagnetic experiment. We note that while STRIP3 produces the most consistent results, there are samples in STRIP1 (Figure 14b) that are also in good agreement with the results from Trindade et al. (2018). This further highlights how the heterogeneity of the stalagmite plays a role in extracting a robust paleomagnetic record, and how nonuniform sampling of the speleothem may help maximize the temporal resolution of the magnetic record.

4.3.3. The Effect of Surface Slope in the Paleomagnetic Record

Between the three samples analyzed here, PD presents the best opportunity to explore how the slope of the growth surface of the speleothem might affect the magnetic record retrieved from these samples. The longitudinal section
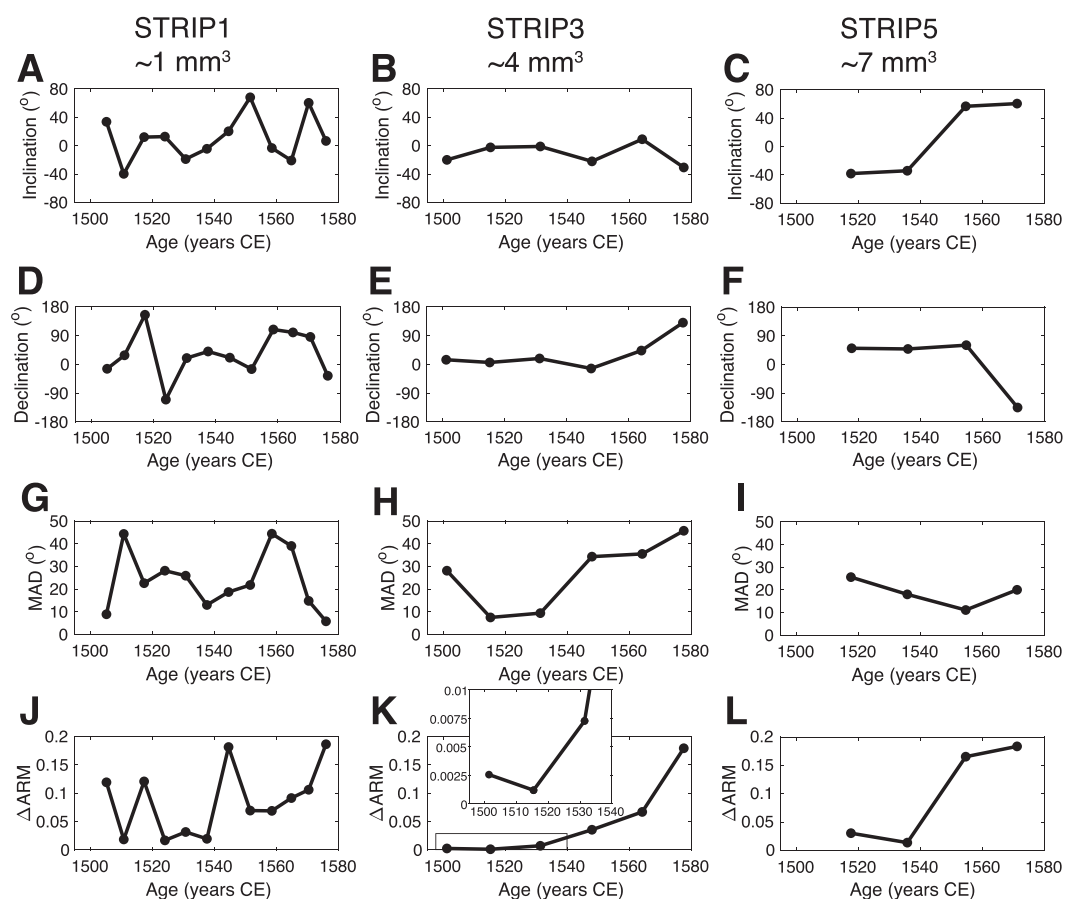
Figure 11. *Summary of magnetic directions, maximum angular deviation (MAD) and ΔARM values as a function of age for the Pau d'Alho (PD) (STRIP1, STRIP3 and STRIP5) samples*. Shown are plots for (a) inclination, (d–f) declination, (g–i) MAD and (j–l) ΔARM. An inset in panel (k) is presented to show the smallest ΔARM values.

of ALHO06 from which we obtained our samples did not originate from an area with horizontal growth layers, but from an area with dipping layers off-center from the central growth axis (Figure 1b). Previous studies have suggested that magnetic records from samples obtained from regions with dipping growth surfaces are not significantly distinct from those that are not horizontal (e.g., Latham et al., 1989; Lean et al., 1995; Morinaga et al., 1989; Openshaw et al., 1997). Nonetheless, a recent study has suggested that this effect might be significant (Ponte et al., 2017). In the case of the stalagmite studied by Ponte et al. (2017), magnetic inclinations increase up to 5° depending on the position of the sample along the flank of the stalagmite. While there is no consistent systematic offset between our data sets and that of the previous study (Figure 14), future work needs to focus on how the slope across a speleothem might affect the magnetic record at finer spatial scales, and micro-paleomagnetism can be used to investigate those questions.

4.4. Dating Speleothems for Micro-Paleomagnetic Studies

Speleothems with higher concentrations of magnetic minerals generally produce better magnetic results. In some cases, this may pose a challenge to the U-Th system used for dating speleothems, as the presence of allochthonous mineral phases that produce the magnetic signal also contaminates the sample with detrital thorium (Lascu & Feinberg, 2011). This suggests that speleothems that are ideal paleomagnetic recorders might not necessarily yield the highest accuracy U-Th dates. The degree to which the allochthonous phases hamper the U/Th dating technique varies on an individual sample basis and reflects a number of variables including the uranium concentration, the ^{232}Th concentration, the degree to which the ^{230}Th/^{232}Th value of the detrital component can be constrained through the application of isochrons, and the sample age. This is best assessed on a case-by-case
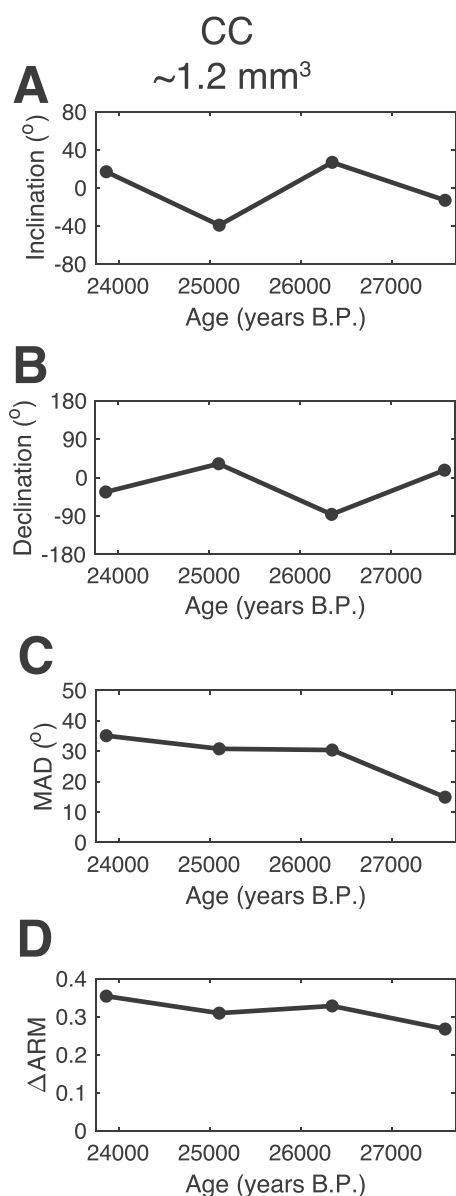
Figure 12. *Summary of magnetic directions, maximum angular deviation (MAD) and ΔARM values as a function of age for the Crevice Cave (CC) samples.* Shown are plots for (a) inclination, (b) declination, (c) MAD and (d) ΔARM.

basis. If the detrital component was introduced by episodic flooding, for example, subsamples for dating can often be carefully extracted from cleaner sections of the stalagmite in between the detrital flood layers. While there are potential ways to date speleothems with high concentration of magnetic minerals (e.g., Trindade et al., 2018), other systems might be able to provide robust ages even when the concentration of magnetic minerals is high. For instance, in cases where uranium is very low, detrital thorium is very high, and the sample is young, such as the LM stalagmite presented in this work, other techniques such as ^{14}C might be utilized to provide chronological control, albeit coming with a set of other limiting factors. Magnetostratigraphic dating could also be potentially used to date speleothems (Oda et al., 2011). Overall, advances in other dating techniques will allow paleomagnetic measurements of speleothems that are ideal for paleomagnetic studies but were not amenable to U-Th dating. One last consideration is that the age spanned by a single sample can be smaller than the uncertainties in the dating process. A possible way to overcome this limitation and assign a more accurate age to each speleothem piece would involve the incorporation of annual layer counting into the age model (Lascu et al., 2016; Trindade et al., 2018).

4.5. How Small Is Too Small?

Our measurements permit us to study the limitations of using small sample sizes to conduct paleomagnetic studies in general. Previous work has proposed that for a millimeter-sized sample to retain a robust thermoremanent magnetization (TRM) record with a 1% accuracy, the sample needs a minimum NRM magnetic moment $>5 \times 10^{-11}$ Am^2 (Berndt et al., 2016; Lima & Weiss, 2016). Our results generally support this estimation as a lower limit, given that the magnetic acquisition mechanism of speleothems is in the form of a DRM and/or CRM, which are less efficient that the TRM. CC samples have NRM values that are an order of magnitude below this number and do not contain enough magnetic carriers to produce robust paleomagnetic results at fine spatial/temporal scales. However, LM samples and some PD samples (e.g., Figure 7a) are below half of this NRM threshold value and still produce reliable magnetic records. Thus, the magnetic moment thresholds of Berndt et al. (2016) seem to be a reasonable proxy for obtaining insights about the magnetic recording ability of a sample.

The potential of obtaining high-resolution paleomagnetic records by targeting samples with excellent magnetic properties, such as LM, can also provide important constrains on secular variation across time. This raises the question: how can we differentiate data scatter, associated with the low concentration of magnetic minerals in these samples, from actual secular variation? For instance, the high-resolution magnetic record of the LM samples reported here to have excellent paleomagnetic properties (Figure 13) show variations in the field of ~20° that could reflect fast secular variation as opposed to scatter associated with the overall lower concentration of magnetic carriers in some of the samples used in this high-resolution study. While a complete description of this observation is outside the scope of this paper, is important to note that such fast variations have been previously reported in the literature (e.g., Chou et al., 2018; Jaqueto et al., 2022; Ponte et al., 2018) and high-resolution paleomagnetism of speleothems might provide important constraints on paleosecular variation at scales that were previously inaccessible while revealing limitations of the magnetic recording processes in speleothems. Ultimately, obtaining robust magnetic records of the actual variation of the field at the geographic location where the speleothem was collected will depend on a combination of the magnetic properties of the speleothem and the position of the samples across the speleothem (i.e., sloped vs. non-sloped). A parameter such as Δ*ARM*, for
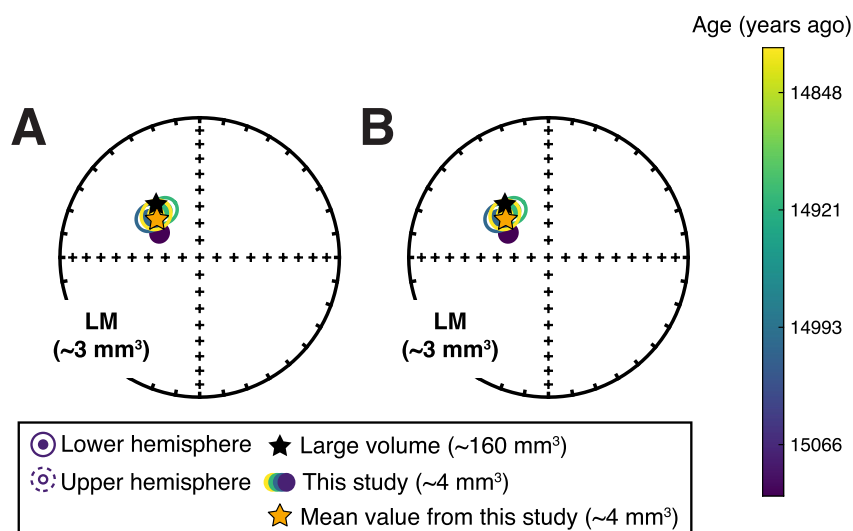
Figure 13. *Comparison between high coercivity directions measured with traditional paleomagnetic techniques and by superconducting quantum interference device (SQUID) microscope for Lapa dos Morcegos (LM) samples.* (a) Equal area stereographic projections showing all directions obtained from LM1. (b) Equal area stereographic projections showing directions with samples that presented $\Delta ARM < 0.047$ from the same samples as (a). No samples were excluded by this selection criterion in this case. Black star is the measurement for this sample using traditional paleomagnetic techniques ($\sim$1,600 mm^3), circles are the SQUID microscope results from this study with color scales indicating the ages of the samples, and yellow star is the average direction of the results from this study.

example, can help provide information about the robustness of the direction obtained from the magnetic record of a sample based on its magnetic properties.

4.6. Workflow for Future Work on Speleothem Micro/Paleomagnetism

We demonstrate that robust records can be obtained from small-volume samples using SQUID microscopy, and we devised the following additional protocols for future studies of micro-paleomagnetism with speleothems to improve accuracy and optimize temporal resolution. First, in the methodology section, we described using non-recycled water during the cutting process of some samples. This is important since sample preparation is key to generally avoid contamination and re-deposition of speleothem particles with random orientations onto the porous surface of the sample that later could negatively impact sample measurements. Given the very small volume of these samples, contamination may easily affect a non-negligible fraction of the moment and result in a larger scatter during NRM demagnetization. Second, repeat AF applications and measurements are beneficial to reduce the uncertainty in the estimation of the magnetic components. Here, we performed a single measurement for a single AF step. For future studies, we recommend using three to five repeat AF applications and moment measurements per AF level to decrease the scatter associated with the AF demagnetization process in speleothems and the low signal-to-noise ratio in some maps. Finally, because some samples might be magnetically hetero-geneous (e.g., PD sample), it is important to start with a NRM map and a test strip to determine which regions of the speleothem can be sampled finer and targeted in higher resolution. An initial SQUID microscope map of a speleothem thick section, such as the ones shown in Figure 4, can be used to discern the regions with higher magnetic signals from which smaller volumes can be extracted. This will help determine which regions have a higher (lower) concentration of magnetic carriers producing finer (coarser) magnetic records across the spe-leothem. Additionally, initial analysis using the SQUID microscope of samples adjacent to the main section of the targeted speleothem can help determine how the speleothem should be subsampled such that the targeted material is adjusted to yield similar small values for ΔARM. For reasonably uniform samples, like the LM stalagmite, such non-uniform sampling/cutting might not be necessary. We also note that cutoffs set by the ΔARM and MAD values are problem-dependent and need to be adjusted according to the question being investigated.
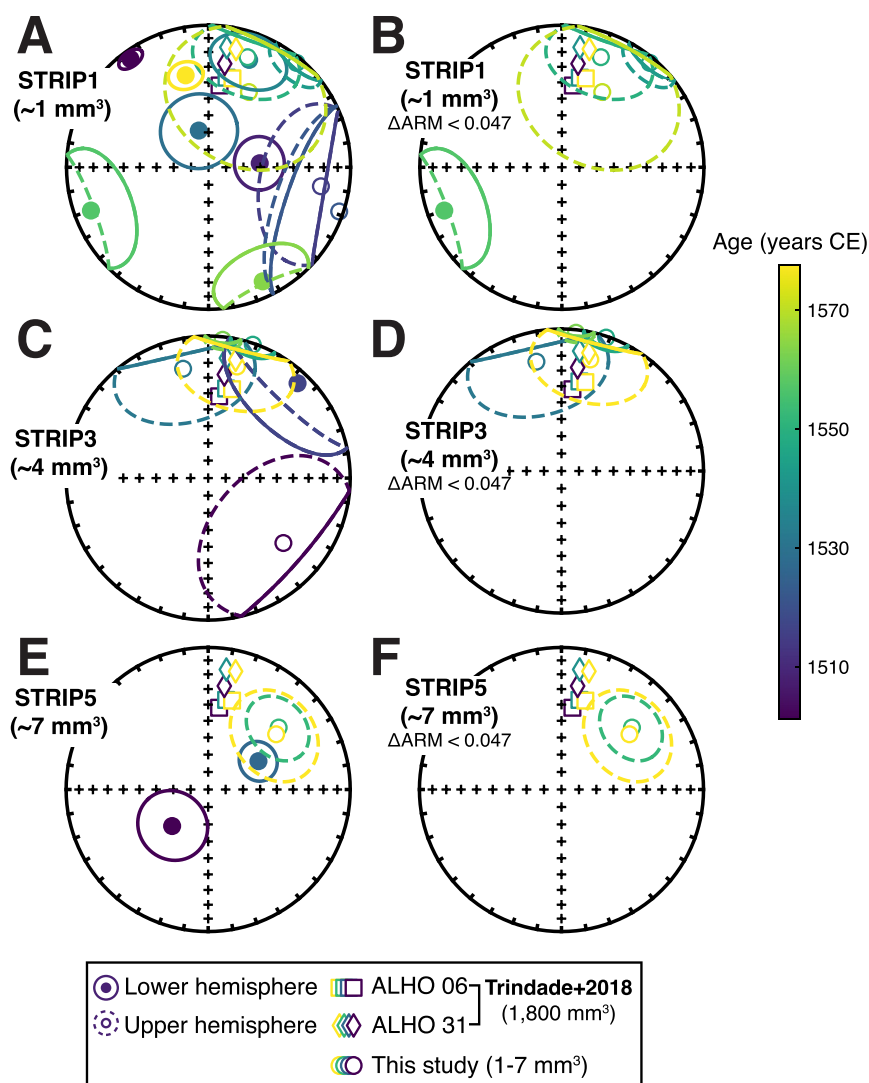
Figure 14. *Comparison between high coercivity directions measured with traditional paleomagnetic techniques and superconducting quantum interference device (SQUID) microscope for Pau d'Alho (PD) samples.* (a, c, e) Equal area stereographic projections showing all directions obtained from STRIP1, STRIP3 and STRIP5, respectively. (b, d, f) Equal area stereographic projections showing directions with samples that presented $\Delta ARM < 0.047$ from the same samples as (a, c, e). Results for Trindade et al. (2018) are shown as squares for ALHO06 and diamonds for ALHO31 (volumes of ~1,800 mm^3). Circles are the SQUID microscope results from this study. Color scales indicate the ages of the samples.

5. Conclusions

We presented paleomagnetic records from three representative speleothems collected from different locations: Lapa dos Morcegos Cave (Portugal), Pau d'Alho Cave (Brazil), and Crevice Cave (USA). We report on the first paleomagnetic study of speleothems using SQUID microscopy targeting small-volume samples to test their feasibility for yielding high-temporal-resolution magnetic records. Overall, we identified that the stalagmite from Lapa dos Morcegos Cave resulted in excellent paleomagnetic data that can improve the temporal resolution of the magnetic records by at least a factor of 5 compared to measurements using traditional paleomagnetic techniques. The speleothem from Pau d'Alho contained magnetic heterogeneities that resulted in paleomagnetic data with varying quality, achieving an improvement in temporal resolution by a factor of up to 3 on average. We recommend that for speleothems with such heterogeneity, a non-uniform sampling strategy be adopted to help optimize the robustness and increase the temporal resolution of the magnetic record. Finally, we show that

samples from Crevice Cave do not have enough magnetic carriers for high-resolution magnetic studies with SQUID microscopy. We discussed how the concentration of magnetic carriers in speleothems limits the smallest sample sizes we can pursue in micro-paleomagnetism studies, and how ^{14}C dating might help us analyze speleothems that otherwise would not be suitable for U-Th dating. We also discussed protocols for future studies that use SQUID microscopy to target speleothems, including initial surveys to identify regions of interest and repeated demagnetization steps to decrease the scatter in the demagnetization data. This study shows that SQUID microscopy can be successfully used to characterize short-term variations of Earth's magnetic field.

Data Availability Statement

The data set for this work can be located in the Magnetics Information Consortium (MagIC) (Borlina et al., 2024).

References

Berndt, T., Muxworthy, A. R., & Fabian, K. (2016). Does size matter? Statistical limits of paleomagnetic field reconstruction from small rock specimens. *Journal of Geophysical Research: Solid Earth*, *121*(1), 15–26. https://doi.org/10.1002/2015jb012441

Borlina, C. S., Lima, E. A., Feinberg, J. M., Jaqueto, P., Lascu, I., Trindade, R. I. F., et al. (2024). Dataset for "Obtaining High-resolution Magnetic Records from Speleothems Using SQUID Microscopy". *Magnetics Information Consortium*. https://doi.org/10.7288/V4/MAGIC/20187

Borlina, C. S., Weiss, B. P., Bryson, J. F. J., Bai, X.-N., Lima, E. A., Chatterjee, N., & Mansbach, E. N. (2021). Paleomagnetic evidence for a disk substructure in the early solar system. *Science Advances*, *7*(42), eabj6928. https://doi.org/10.1126/sciadv.abj6928

Borlina, C. S., Weiss, B. P., Lima, E. A., Tang, F., Taylor, R. J. M., Einsle, J. F., et al. (2020). Reevaluating the evidence for a Hadean-Eoarchean dynamo. *Science Advances*, *6*(15), eaav9634. https://doi.org/10.1126/sciadv.aav9634

Chou, Y.-M., Jiang, X., Liu, Q., Hu, H.-M., Wu, C.-C., Liu, J., et al. (2018). Multidecadally resolved polarity oscillations during a geomagnetic excursion. *Proceedings of the National Academy of Sciences*, *115*(36), 8913–8918. https://doi.org/10.1073/pnas.1720404115

Egli, R. (2013). VARIFORC: An optimized protocol for calculating non-regular first-order reversal curve (FORC) diagrams. *Global and Planetary Change*, *110*, 302–320. https://doi.org/10.1016/j.gloplacha.2013.08.003

Egli, R., & Heller, F. (2000). High-resolution imaging using a high-T$_c$ superconducting quantum interference device (SQUID) magnetometer. *Journal of Geophysical Research*, *105*(B11), 25709–25727. https://doi.org/10.1029/2000jb900192

Feinberg, J. M., Lascu, I., Lima, E. A., Weiss, B. P., Dorale, J. A., Alexander, E. C., & Edwards, R. L. (2020). Magnetic detection of paleoflood layers in stalagmites and implications for historical land use changes. *Earth and Planetary Science Letters*, *530*, 115946. https://doi.org/10.1016/j.epsl.2019.115946

Fischer, W. W., Fike, D. A., Johnson, J. E., Raub, T. D., Guan, Y., Kirschvink, J. L., & Eiler, J. M. (2014). SQUID–SIMS is a useful approach to uncover primary signals in the Archean sulfur cycle. *Proceedings of the National Academy of Sciences*, *111*(15), 5468–5473. https://doi.org/10.1073/pnas.1322577111

Fong, L. E., Holzer, J. R., McBride, K. K., Lima, E. A., Baudenbacher, F., & Radparvar, M. (2005). High-resolution room-temperature sample scanning superconducting quantum interference device microscope configurable for geological and biomagnetic applications. *Review of Scientific Instruments*, *76*(5), 053703. https://doi.org/10.1063/1.1884025

Font, E., Veiga-Pires, C., Pozo, M., Carvallo, C., de Siqueira Neto, A. C., Camps, P., et al. (2014). Magnetic fingerprint of southern Portuguese speleothems and implications for paleomagnetism and environmental magnetism. *Journal of Geophysical Research: Solid Earth*, *119*(11), 7993–8020. https://doi.org/10.1002/2014jb011381

Fu, R. R., Hess, K., Jaqueto, P., Novello, V. F., Kukla, T., Trindade, R. I. F., et al. (2021). High-resolution environmental magnetism using the Quantum Diamond Microscope (QDM): Application to a tropical speleothem. *Frontiers in Earth Science*, *8*, 604505. https://doi.org/10.3389/feart.2020.604505

Fu, R. R., Lima, E. A., & Weiss, B. P. (2014). No nebular magnetization in the Allende CV carbonaceous chondrite. *Earth and Planetary Science Letters*, *404*, 54–66. https://doi.org/10.1016/j.epsl.2014.07.014

Fu, R. R., Weiss, B. P., Lima, E. A., Harrison, R. J., Bai, X.-N., Desch, S. J., et al. (2014). Solar nebula magnetic fields recorded in the Semarkona meteorite. *Science*, *346*(6213), 1089–1092. https://doi.org/10.1126/science.1258022

Fu, R. R., Weiss, B. P., Lima, E. A., Kehayias, P., Araujo, J. F. D. F., Glenn, D. R., et al. (2017). Evaluating the paleomagnetic potential of single zircon crystals using the Bishop Tuff. *Earth and Planetary Science Letters*, *458*, 1–13. https://doi.org/10.1016/j.epsl.2016.09.038

Harrison, R. J., & Feinberg, J. M. (2008). FORCinel: An improved algorithm for calculating first-order reversal curve distributions using locally weighted regression smoothing. *Geochemistry, Geophysics, Geosystems*, *9*(5), Q01056. https://doi.org/10.1029/2008gc001987

Harrison, R. J., & Lascu, I. (2014). FORCulator: A micromagnetic tool for simulating first-order reversal curve diagrams. *Geochemistry, Geophysics, Geosystems*, *15*(12), 4671–4691. _eprint. https://doi.org/10.1002/2014GC005582

Jaqueto, P., Trindade, R. I. F., Hartmann, G. A., Novello, V. F., Cruz, F. W., Karmann, I., et al. (2016). Linking speleothem and soil magnetism in the Pau d'Alho cave (central South America). *Journal of Geophysical Research: Solid Earth*, *121*(10), 7024–7039. https://doi.org/10.1002/2016jb013541

Jaqueto, P., Trindade, R. I. F., Terra-Nova, F., Feinberg, J. M., Novello, V. F., Stríkis, N. M., et al. (2022). Stalagmite paleomagnetic record of a quiet mid-to-late Holocene field activity in central South America. *Nature Communications*, *13*(1), 1349. https://doi.org/10.1038/s41467-022-28972-8

Kirschvink, J. L. (1980). The least-squares line and plane and the analysis of paleomagnetic data: Examples from Siberia and Morocco. *Geophysical Journal International*, *62*(3), 699–718. https://doi.org/10.1111/j.1365-246x.1980.tb02601.x

Kirschvink, J. L., Kopp, R. E., Raub, T. D., Baumgartner, C. T., & Holt, J. W. (2008). Rapid, precise, and high-sensitivity acquisition of paleomagnetic and rock-magnetic data: Development of a low-noise automatic sample changing system for superconducting rock magnetometers. *Geochemistry, Geophysics, Geosystems*, *9*(5), 1–18. https://doi.org/10.1029/2007gc001856

Lascu, I., Einsle, J. F., Ball, M. R., & Harrison, R. J. (2018). The Vortex State in geologic materials: A micromagnetic perspective. *Journal of Geophysical Research: Solid Earth*, *123*(9), 7285–7304. _eprint. https://doi.org/10.1029/2018JB015909

Lascu, I., & Feinberg, J. M. (2011). Speleothem magnetism. *Quaternary Science Reviews*, *30*(23), 3306–3320. https://doi.org/10.1016/j.quascirev.2011.08.004

Lascu, I., Feinberg, J. M., Dorale, J. A., Cheng, H., & Edwards, R. L. (2016). Age of the Laschamp excursion determined by U-Th dating of a speleothem geomagnetic record from North America. *Geology*, *44*(2), 139–142. https://doi.org/10.1130/g37490.1

Latham, A. G., Ford, D. C., Schwarcz, H. P., & Birchall, T. (1989). Secular variation from Mexican stalagmites: Their potential and problems. *Physics of the Earth and Planetary Interiors*, *56*(1), 34–48. https://doi.org/10.1016/0031-9201(89)90034-4

Latham, A. G., Schwarcz, H. P., Ford, D. C., & Pearce, G. W. (1979). Palaeomagnetism of stalagmite deposits. *Nature*, *280*(5721), 383–385. https://doi.org/10.1038/280383a0

Lean, C. B., Latham, A. G., & Shaw, J. (1995). Palaeosecular variation from a Vancouver Island stalagmite and comparison with contemporary North American records. *Journal of Geomagnetism and Geoelectricity*, *47*(1), 71–87. https://doi.org/10.5636/jgg.47.71

Lima, E. A., & Weiss, B. P. (2016). Ultra-high sensitivity moment magnetometry of geological samples using magnetic microscopy. *Geochemistry, Geophysics, Geosystems*, *17*(9), 3754–3774. https://doi.org/10.1002/2016gc006487

Lima, E. A., Weiss, B. P., Borlina, C. S., Baratchart, L., & Hardin, D. P. (2023). Estimating the net magnetic moment of geological samples from planar field maps using multipoles. *Geochemistry, Geophysics, Geosystems*, *24*(7), e2022GC010724. https://doi.org/10.1029/2022gc010724

Morinaga, H., Inokuchi, H., & Yaskawa, K. (1985). Paleomagnetism and paleotemperature of a stalagmite. *Journal of Geomagnetism and Geoelectricity*, *37*(8), 823–828. https://doi.org/10.5636/jgg.37.823

Morinaga, H., Inokuchi, H., & Yaskawa, K. (1989). Palaeomagnetism of stalagmites (speleothems) in SW Japan. *Geophysical Journal International*, *96*(3), 519–528. https://doi.org/10.1111/j.1365-246x.1989.tb06011.x

Novello, V. F., Vuille, M., Cruz, F. W., Stríkis, N. M., de Paula, M. S., Edwards, R. L., et al. (2016). Centennial-scale solar forcing of the South American Monsoon System recorded in stalagmites. *Scientific Reports*, *6*(1), 24762. https://doi.org/10.1038/srep24762

Oda, H., Kawai, J., Miyamoto, M., Miyagi, I., Sato, M., Noguchi, A., et al. (2016). Scanning SQUID microscope system for geological samples: System integration and initial evaluation. *Earth, Planets and Space*, *68*(1), 179. https://doi.org/10.1186/s40623-016-0549-3

Oda, H., Usui, A., Miyagi, I., Joshima, M., Weiss, B. P., Shantz, C., et al. (2011). Ultrafine-scale magnetostratigraphy of marine ferromanganese crust. *Geology*, *39*(3), 227–230. https://doi.org/10.1130/g31610.1

Openshaw, S., Latham, A., & Shaw, J. (1997). Speleothem palaeosecular variation records from China: Their contribution to the coverage of Holocene palaeosecular variation data in East Asia. *Journal of Geomagnetism and Geoelectricity*, *49*(4), 485–505. https://doi.org/10.5636/jgg.49.485

Ponte, J. M., Font, E., Veiga-Pires, C., & Hillaire-Marcel, C. (2018). Speleothems as magnetic archives: Paleosecular variation and a relative paleointensity record from a Portuguese speleothem. *Geochemistry, Geophysics, Geosystems*, *19*(9), 2962–2972. https://doi.org/10.1029/2018gc007651

Ponte, J. M., Font, E., Veiga-Pires, C., Hillaire-Marcel, C., & Ghaleb, B. (2017). The effect of speleothem surface slope on the remanent magnetic inclination. *Journal of Geophysical Research: Solid Earth*, *122*(6), 4143–4156. https://doi.org/10.1002/2016jb013789

Ramsey, C. B. (2009). Bayesian analysis of radiocarbon dates. *Radiocarbon*, *51*(1), 337–360. https://doi.org/10.1017/s0033822200033865

Reimer, P. J., Austin, W. E. N., Bard, E., Bayliss, A., Blackwell, P. G., Ramsey, C. B., et al. (2020). The IntCal20 Northern Hemisphere radiocarbon age calibration curve (0–55 cal kBP). *Radiocarbon*, *62*(4), 725–757. https://doi.org/10.1017/rdc.2020.41

Roberts, A. P., Almeida, T. P., Church, N. S., Harrison, R. J., Heslop, D., Li, Y., et al. (2017). Resolving the origin of pseudo-single domain magnetic behavior. *Journal of Geophysical Research: Solid Earth*, *122*(12), 9534–9558. _eprint. https://doi.org/10.1002/2017JB014860

Sánchez-Moreno, E. M., Font, E., Pavón-Carrasco, F. J., Dimuccio, L. A., Hillaire-Marcel, C., Ghaleb, B., & Cunha, L. (2022). Paleomagnetic techniques can date speleothems with high concentrations of detrital material. *Scientific Reports*, *12*(1), 17936. https://doi.org/10.1038/s41598-022-21761-9

Strauss, B. E., Strehlau, J. H., Lascu, I., Dorale, J. A., Penn, R. L., & Feinberg, J. M. (2013). The origin of magnetic remanence in stalagmites: Observations from electron microscopy and rock magnetism. *Geochemistry, Geophysics, Geosystems*, *14*(12), 5006–5025. https://doi.org/10.1002/2013gc004950

Tauxe, L., & Staudigel, H. (2004). Strength of the geomagnetic field in the Cretaceous Normal Superchron: New data from submarine basaltic glass of the Troodos Ophiolite. *Geochemistry, Geophysics, Geosystems*, *5*(2), Q02H06. https://doi.org/10.1029/2003gc000635

Trindade, R. I. F., Jaqueto, P., Terra-Nova, F., Brandt, D., Hartmann, G. A., Feinberg, J. M., et al. (2018). Speleothem record of geomagnetic South Atlantic Anomaly recurrence. *Proceedings of the National Academy of Sciences*, *115*(52), 13198–13203. https://doi.org/10.1073/pnas.1809197115

Weiss, B. P., Lima, E. A., Fong, L. E., & Baudenbacher, F. J. (2007). Paleomagnetic analysis using SQUID microscopy. *Journal of Geophysical Research*, *112*(B9), B09105. https://doi.org/10.1029/2007jb004940

Yokoyama, Y., Miyairi, Y., Aze, T., Sawada, C., Ando, Y., Izawa, S., et al. (2022). Efficient radiocarbon measurements on marine and terrestrial samples with single stage Accelerator Mass Spectrometry at the Atmosphere and Ocean Research Institute, University of Tokyo. *Nuclear Instruments and Methods in Physics Research Section B: Beam Interactions with Materials and Atoms*, *532*, 62–67. https://doi.org/10.1016/j.nimb.2022.10.006

Yokoyama, Y., Miyairi, Y., Aze, T., Yamane, M., Sawada, C., Ando, Y., et al. (2019). A single stage Accelerator Mass Spectrometry at the Atmosphere and Ocean Research Institute, The University of Tokyo. *Nuclear Instruments and Methods in Physics Research Section B: Beam Interactions with Materials and Atoms*, *455*, 311–316. https://doi.org/10.1016/j.nimb.2019.01.055

Yokoyama, Y., Miyairi, Y., Matsuzaki, H., & Tsunomori, F. (2007). Relation between acid dissolution time in the vacuum test tube and time required for graphitization for AMS target preparation. *Nuclear Instruments and Methods in Physics Research Section B: Beam Interactions with Materials and Atoms*, *259*(1), 330–334. https://doi.org/10.1016/j.nimb.2007.01.176

Zhu, Z. M., Feinberg, J. M., Xie, S. C., Bourne, M. D., Huang, C. J., Hu, C. Y., & Cheng, H. (2017). Holocene ENSO-related cyclic storms recorded by magnetic minerals in speleothems of central China. *Proceedings of the National Academy of Sciences*, *114*(5), 852–857. https://doi.org/10.1073/pnas.1610930114

Zhu, Z. M., Zhang, S., Tang, C., Li, H., Xie, S., Ji, J., & Xiao, G. (2012). Magnetic fabric of stalagmites and its formation mechanism. *Geochemistry, Geophysics, Geosystems*, *13*(6), Q06006. https://doi.org/10.1029/2011gc003869